DOI: 10.1002/ejic.200901015

Mg-Assisted Autoclave Synthesis of RB_6 (R = Sm, Eu, Gd, and Tb) Submicron Cubes and SmB_6 Submicron Rods

Maofeng Zhang,*[a,b] Ying Jia,[a] Guogen Xu,[a] Pengfei Wang,[b] Xiaoqing Wang,[b] Shenglin Xiong,[b] Xuanjun Wang,[a] and Yitai Qian*[b]

Keywords: Rare earths / Hexaborides / Magnesium / Solid-state reactions / Crystal growth

Submicron crystalline rare-earth hexaborides (RB_6; R = Sm, Eu, Gd, and Tb) have been successfully prepared by a facile one-step solid-state reaction of $RCl_3 \cdot 6H_2O$, B_2O_3, and Mg powder in an autoclave at the relatively low temperature of 500 °C. By controlling the reaction conditions, submicron-sized cubes (RB_6) and rod- and needlelike SmB_6 are obtained. The possible growth mechanism of the 1D SmB_6 structures has also been discussed. The XRD patterns of the products show that all of the hexaborides can be indexed to a cubic phase with high crystallinity and high purity. The field-emission scanning electron microscopy (FESEM) and TEM images display their cube-, rod-, and needlelike morphologies. The selected-area electron diffraction (SAED) patterns reveal the single-crystalline nature of the products.

Introduction

Rare-earth hexaborides have attracted much attention because of their various peculiar properties such as high melting point, high hardness, high chemical stability, superconductivity,[1,2] magnetic properties,[3–5] high efficiency thermionic emission, and narrow-band semiconductivity, and so forth.[6–10] Therefore, rare-earth hexaborides have great technical importance and their synthesis is significant.

Most previous methods for the preparation of rare-earth hexaborides need either high temperature or harsh reaction conditions, such as the direct solid-phase reaction of a lanthanide or its oxides with elemental boron at around 1800 °C;[1,11–13] the floating-zone method of rare-earth oxides with boron at 1700 °C;[5,14,15] the high-pressure and high-temperature synthesis from rare-earth oxides and boron at 1600 °C;[16] the carbothermal reduction of lanthanide oxide and boron at 1500 °C;[17] the solution method in molten aluminum at about 1300 °C;[18] and the chemical vapor deposition (CVD) method at around 1150 °C.[7,8,19] However, there are only a few papers reporting the synthesis of hexaborides below 1000 °C. For example, LaB_6 crystals were synthesized from molten-salt electrolysis at 850 °C.[20] Also, LaB_6 thin films were deposited by using the pulsed-laser deposition (PLD) technique at 850 °C.[21] Recently, submicron-sized rare-earth hexaborides were synthesized at 900 °C using metal acetate precursors.[22] Since the properties of a material can be significantly changed by their particle size due to quantum effects, itis expected that microstructured RB_6, such as nanowires[7,8,23] and nanoobelisks,[24] can give rise to exceptional properties. In short, because hexaborides are of great technological importance, researchers are trying to explore low reaction temperature, low cost, and simple and convenient synthetic methods for the preparation of these microstructured compounds.

Following these demands, we have recently proposed and adopted the simple and novel technique of Mg-assisted autoclave solid-state reactions (reaction under autogenic pressure at elevated temperature). By using this method, rare-earth hexaborides with the general formula of RB_6 (R = La, Ce, Pr, and Nd) consisting of nanocubes and nanoparticles have been successfully synthesized in the temperature range from 400 to 500 °C.[25] In the present study, we extend the synthetic method of LaB_6 nanocubes and nanoparticles[26] to the preparation of RB_6 (R = Sm, Eu, Gd, and Tb) submicron materials, using cheap and easily available metal chloride precursors, B_2O_3, and metallic magnesium powder as the raw materials. It is unique that the present work produced 1D hexaborides, which is different from our previous work. The structure and morphologies of the products have been characterized by means of X-ray diffraction (XRD), selected-area electron diffraction (SAED), field-emission scanning electron microscopy (FESEM), transmission electron microscopy (TEM), and high-resolution transmission electron microscopy (HRTEM). To the best of our knowledge, no such study has ever been reported on the low-temperature, low-cost, and simple chemical synthesis of 1D hexaborides.

[a] Section 503, Xi'an High Technique Institute,
Xi'an 710025, P. R. China
E-mail: mfzhang@ustc.edu.cn
[b] Hefei National Laboratory for Physical Sciences at the Microscale and Department of Chemistry, University of Science and Technology of China,
Hefei 230026, P. R. China
E-mail: ytqian@ustc.edu.cn

Results and Discussion

The crystal structures and the phase purity of the materials were determined by XRD. Typical XRD patterns of the SmB_6, EuB_6, GdB_6, and TbB_6 products are presented in Figure 1. The strong and sharp reflection peaks reveal that the as-prepared materials are highly crystalline. The diffraction peaks were carefully indexed and assigned to the lattice planes of (100), (110), (111), (200), (210), (211), (220), (300), (310), and (311) for the corresponding "*d*" spacings. All the peaks can be readily indexed to a cubic crystal system [space group: *Pm3m* (221)] of hexaborides with calculated lattice constants (*a*) of (4.133±0.001) Å (SmB_6), (4.190±0.001) Å (EuB_6), (4.107±0.001) Å (GdB_6), and (4.105±0.001) Å (TbB_6), which are very close to the reported data (JCPDS card nos.: 24-1120, 40-1308, 24-1082, 25-0932). No other impurity peaks of B, MgO, or B_2O_3 were detected, which indicates the high purity of the as-obtained samples.

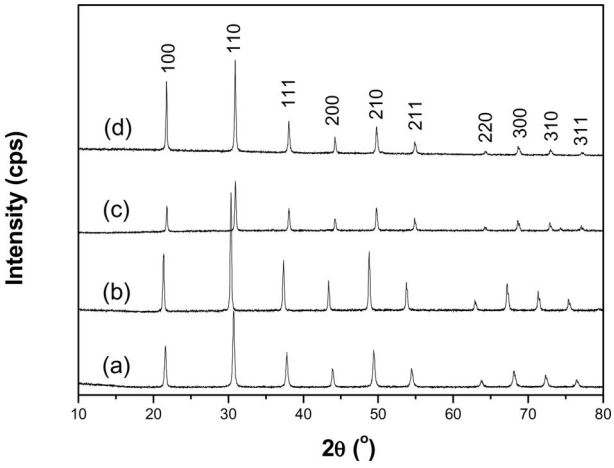

Figure 1. XRD patterns of the as-prepared products (a) SmB_6, (b) EuB_6, (c) GdB_6, and (d) TbB_6.

The Formation of Hexaboride Submicron Cubes

The morphologies and microstructure of the samples were examined by FESEM. Figure 2 shows the FESEM images of hexaborides prepared at 500 °C for 12 h. It is evident that all the products have a cubic morphology. The particle size distribution for SmB_6 and EuB_6 samples ranges from approximately 150 nm to approximately 400 nm, as obtained by measuring the size of a large number of well-defined particles. However, GdB_6 and TbB_6 crystals show more or less uniform-sized particles with particle size ranges from approximately 300 nm to approximately 500 nm. For TbB_6 crystals, in addition to the submicron cubes, some nanoparticle structure is also observed on the surface of the as-obtained products.

Figure 3 shows TEM images of the as-prepared hexaborides. The images confirm that the hexaborides have a cubic morphology, which is consistent with the FESEM results. Figure 3 (a) shows a TEM image of a SmB_6 sample. The calculated average particle size of SmB_6 is about 200 nm, and the SAED pattern (inset) reveals the single-crystalline nature of individual SmB_6 submicron cubes. An average particle size of about approximately 200 nm is observed in Figure 3 (b) for EuB_6 crystals, and it clearly shows the 3D nature of a single crystal. Similarly, GdB_6 and TbB_6 crystals (Figure 3, c and d) have the same cubic morphology with an average particle size of about 400 nm. By a series of detailed temperature- and time-dependent experiments, it was found that a large amount of RB_6 submicron cubes can be obtained under the optimum reaction conditions of 500 °C for 12 h.

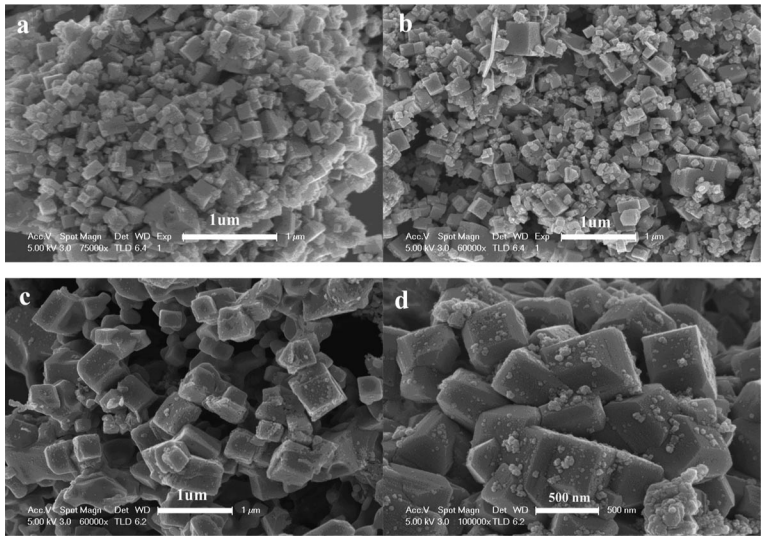

Figure 2. FESEM images of the as-prepared (a) SmB_6, (b) EuB_6, (c) GdB_6, and (d) TbB_6.

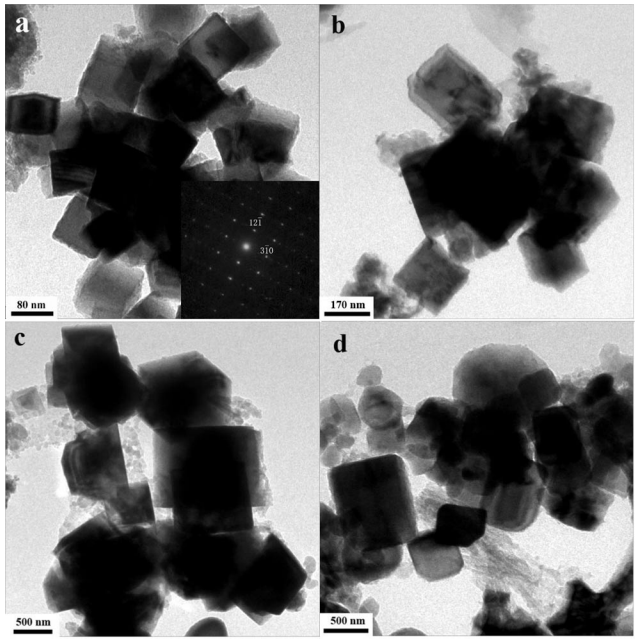

Figure 3. TEM images of the as-prepared (a) SmB_6 (inset: corresponding SAED patterns), (b) EuB_6, (c) GdB_6, and (d) TbB_6.

The Formation of 1D Rod- and Needlelike Hexaboride

In the present preparation process, it was found that the reaction time plays an important role in the formation of 1D hexaborides. To reveal the intermediate steps in the formation of the 1D structure, a series of detailed time-dependent experiments was carried out at 500 °C. For SmB_6 samples, if the reaction time was shorter than 4 h, the reaction was very incomplete and the crystallinity of the product was very poor due to the reaction time being too short. When the reaction time was 12 h, the initial poorly crystalline products turned into highly crystalline submicron cubes (Figure 3, a). However, when the reaction time was 24 h, the products became rodlike. The size and morphology of the as-prepared SmB_6 samples were examined using FESEM, TEM, SAED, and HRTEM. Typical images of the SmB_6 samples are shown in parts a–d of Figure 4. Figure 4 (a) clearly reveals a highly monodisperse distribution of a rodlike structure that has a width of approximately 150–250 nm and a mean length of approximately 1.5 μm. Figure 4 (b) shows the TEM image of a single rod, which clearly discloses the cubic pillar structure morphology. The SAED pattern (Figure 4, c) reveals the single-crystalline na-

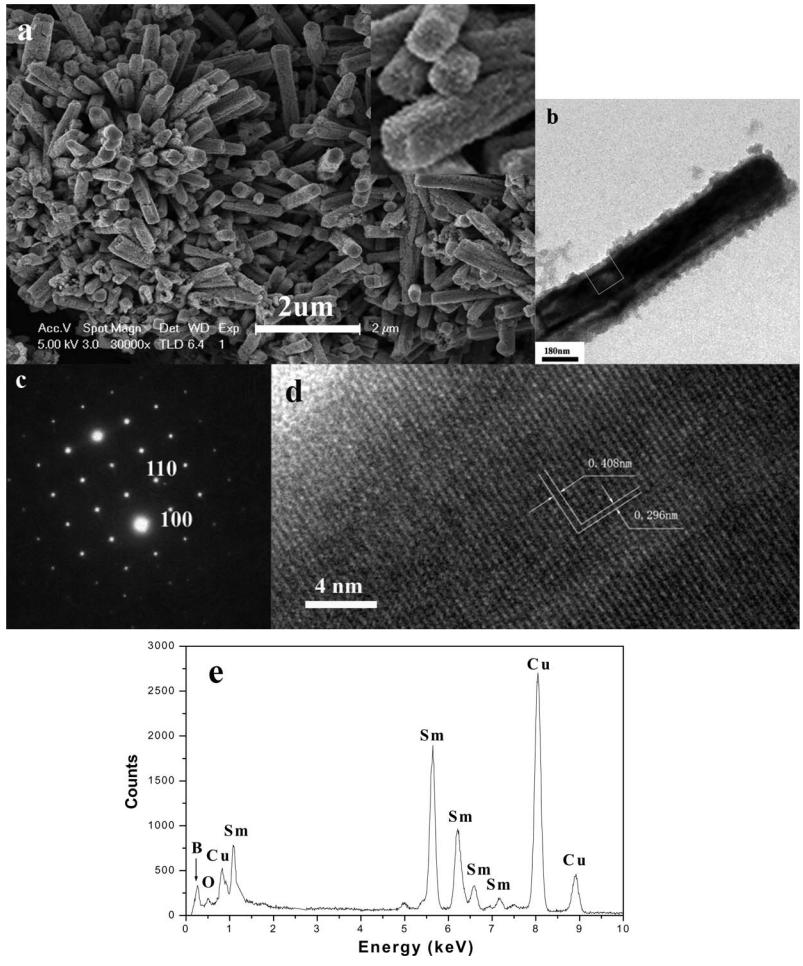

Figure 4. (a) FESEM (the inset shows an enlarged image), (b) TEM, (c) SAED, and (d) HRTEM images, and (e) an EDX spectrum of rodlike SmB_6 samples prepared at 500 °C for 24 h.

ture of a single rod with a preferential growth direction along the long axis direction. The HRTEM image (Figure 4, d) shows that the rodlike SmB_6 are structurally uniform with interplanar spacings of about 0.408 and 0.296 nm, which correspond to the (100) and (110) lattice spacings of SmB_6, respectively. This structural information indicated that the growth direction of the sample shown in Figure 4 (b) was in the <001> direction. It is noteworthy that the SEM and TEM images were obtained from randomly selected areas of the sample and, as such, are representative of the overall shapes and sizes of our as-prepared SmB_6 submicron rods. Energy-dispersive X-ray (EDX) spectroscopy was also used to characterize the composition of the products. EDX analysis of the SmB_6 submicron rods revealed the presence of Sm and B (Figure 4, e), both of which are dominant in the materials. The other elements detected in the samples originate from copper grids and the absorption of oxygen on the powder surface. By comparing a series of experiments, it is concluded that the optimum reaction conditions for large-scale preparation of rodlike SmB_6 are 500 °C for 24 h. However, surfaces of as-synthesized 1D SmB_6 submicron crystals are not very regular (shown in the inset of Figure 4, a). Because the products were prepared by means of a solid-state reaction, the surfaces of the products were not easy to control. If the reaction temperature is reduced to around 400 °C, it can be carried out in a benzene–thermal reaction system, and smooth surfaces of the products are then available. Much work is needed and the relevant research is under way.

With further extension of the reaction time from 24 to 48 h, the products gradually transformed from rod- to needlelike in structure. As shown in Figure 5 (a), rodlike SmB_6 partly turned into a needlelike structure after it had reacted for 36 h. After 48 h, needlelike SmB_6 with needle lengths of up to 2 μm were formed (Figure 5, b). It was found that the lengths of the needles are longer than the lengths of the rods. This is due to the persistent, oriented growth of the incomplete product rods. The reaction temperature is another key factor in the formation of 1D structures of RB_6. For example, at the lower temperature of 450 °C, only a small amount of RB_6 submicron cubes and nanoparticles could be obtained. However, needlelike SmB_6 was fabricated at the elevated reaction temperature of 600 °C, as shown in Figure 5 (c).

The Growth Process and Mechanism of 1D Hexaborides

To substantially understand the growth mechanism of the 1D hexaborides under the present synthetic route, we have systematically surveyed the growth process by analyzing the 1D structure of the hexaborides at different stages. The whole growth process of the 1D structure can be schematically illustrated as shown in Figure 6. Firstly, it produced an amorphous product. This amorphous product acted as the nucleation center for the formation of hexaboride submicron cubes. At the elevated temperature of 500 °C, it was converted into small crystalline primary particles (Figure 6, a). Secondly, following a 3D-oriented attachment,[27] the crystalline primary particles were transformed into imperfect submicron cubes after an 8 h reaction (Figure 6, b). Thirdly, when the reaction proceeded for 12 h, the perfect submicron cubes were obtained (Figure 6, c). This was due to the so-called Ostwald ripening process,[28] in which the large particles grew at the cost of the small ones through the diffusion of ions, atoms, or molecules within an assembly of crystallites. Fourthly, as the reaction time was further prolonged to 24 h, the submicron cubes grew through an oriented attachment process,[29–32] in which the adjacent particles are self-assembled by sharing a common crystallographic orientation and docking of these particles at a planar interface. They firstly transformed to short rods (Figure 6, d) and then long rods (Figure 6, e). Finally, after the reaction had proceeded for long enough (48 h), the needlelike structure started to predominate in the products through a transformation process using the

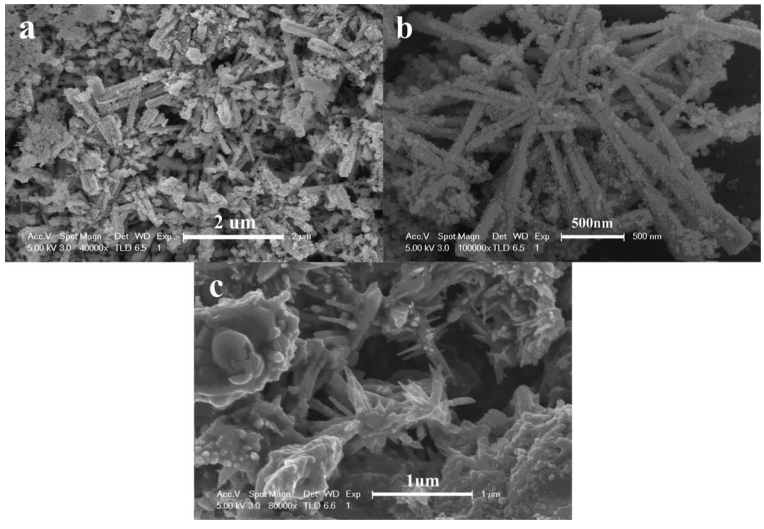

Figure 5. FESEM images of SmB_6 samples prepared at (a) 500 °C for 36 h, (b) 500 °C for 48 h, and (c) 600 °C for 24 h.

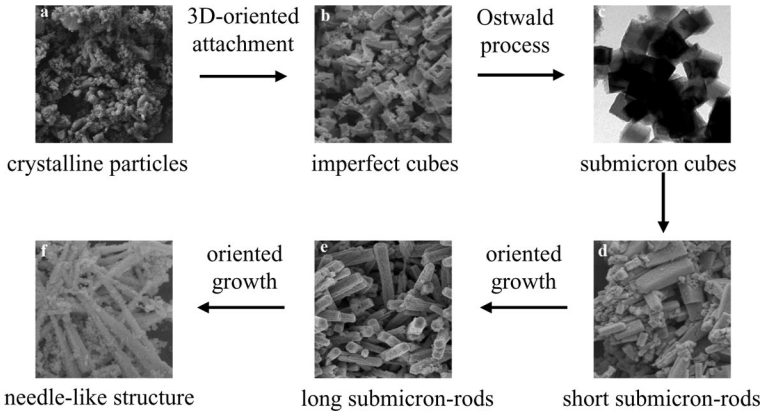

Figure 6. Schematic illustration of the growth process of the 1D SmB_6.

irregular particles as precursors (Figure 6, f). It is clear that the crystalline phase of the nuclei is critical for directing the intrinsic shapes of the crystals due to its characteristic symmetry and structure.

On the basis of the above experimental observations, we believe that the present 1D RB_6 structures were produced by a Mg-assisted co-reduction growth mechanism. That is to say, during the formation process of the 1D hexaboride structures, Mg acted as a reducing agent. The reaction [Equations (1), (2), (3), and (4)] can be described as follows:

$$RCl_3{\cdot}6H_2O(s) + 3B_2O_3(s) + 16.5Mg(s) \rightarrow RB_6(s) + 1.5MgCl_2(s) + 15MgO(s) + 6H_2(g) \quad (1)$$

$$B_2O_3(s) + 3Mg(s) \rightarrow 2B(s) + 3MgO(s) \quad (2)$$

$$2RCl_3(s) + 3Mg(s) \rightarrow 2R(s) + 3MgCl_2(s) \quad (3)$$

$$R(s) + 6B(s) \rightarrow RB_6(s) \quad (4)$$

This reaction [Equation (1)] is thermodynamically spontaneous and exothermic ($\Delta_r H_m^{\Theta} = -3656.1\ kJ\,mol^{-1}$). Though the present reaction temperature (500 °C) is lower than the melting point of Mg (648 °C), the Mg powder will partly transform from the solid state to the liquid state because of the heat of the reaction that is generated. In the preparation of hexaborides, as Equation (1) describes, B_2O_3 begins to turn to liquid (melting point 450 °C) in the heating process. With the increase of temperature, more liquid B_2O_3 coats the Mg and is reduced to B atoms [Equation (2)]. When RCl_3 makes contact with the Mg, it is reduced to R atoms [Equation (3)]. The fresh B and R atoms have a higher activity than commercial boron and rare-earth-metal elements, which enables the formation of RB_6 submicron cubes at the low temperature of 500 °C [Equation (4)]. At the same time, the fast transport of the RB_6 species in the high-pressure environment, arising from the H_2 produced during the reaction {about 50 atm [Equation (1)], estimated by the ideal gas law}, might be responsible for the growth of the highly crystalline RB_6 1D structures. However, as it is difficult to monitor the reaction once the system is sealed, much work needs to be done to investigate the kinetics of the reaction.

Conclusion

In summary, we have developed a facile and straightforward synthetic method to prepare hexaboride submicron cubes and 1D rod- and needlelike structures at the low temperature of 500 °C. The XRD and SAED patterns confirm the high crystallinity, high purity, and the single-crystalline nature of the products. The FESEM and TEM images clearly show their cube-, rod-, and needlelike morphologies. The possible growth mechanism of the 1D structured RB_6 has also been discussed. The present route has the advantages of mildness, simplicity, and low cost, so we believe that this approach might be applied to the synthesis of a new generation of important metal hexaborides.

Experimental Section

Sample Preparation: All of the chemical reagents (Analytical Grade) used in this experiment were purchased from National Reagent Corporation (Shanghai, China) and used without further purification. In a typical procedure, an appropriate amount of $RCl_3{\cdot}6H_2O$ (0.003 mol), B_2O_3 (0.009 mol), and an excess amount of Mg (0.075 mol) were put into a stainless steel autoclave of 25 mL capacity. Then, the autoclave was sealed under an Ar atmosphere in a glove box and was maintained at 500 °C for 12 to 48 h, followed by being left to cool to room temperature. The products were washed with dilute hydrochloric acid (4 mol L^{-1}), absolute ethanol, and distilled water several times, respectively, to remove MgO, $MgCl_2$, and other impurities. The final products were vacuum-dried at 60 °C for 6 h.

Characterization: The phase and composition of the products were determined by a Rigaku D/Max-γA rotating-anode X-ray diffractometer equipped with monochromatic high-intensity Cu-K_α radiation (λ = 1.54178 Å). The morphologies of the samples were observed with a transmission electron microscope (JEOL-2010) with an attached EDX system, which had an accelerating voltage of 200 kV with a tungsten filament. FESEM images were recorded on a JEOL JSM-6300F SEM instrument.

Acknowledgments

This work was supported by the National Natural Science Foundation of China (no. 20431020), the 973 Project of China (no.

2005CB623601), the China Postdoctoral Science Foundation Funded Project (no. 20080440708), and the Natural Science Basic Research Plan in Shaanxi Province of China (no. 2009JQ2012).

[1] K. Hiebl, M. J. Sienko, *Inorg. Chem.* **1980**, *19*, 2179–2180.
[2] I. Bat'Ko, M. Bat'Kova, K. Flachbart, *J. Alloys Compd.* **1995**, *217*, L1–L3.
[3] H. Hacker, Y. Shimada, K. S. Chung, *Physica Status Solidi A* **1970–1996**, *4*, 459–462.
[4] J. R. Shannon, M. J. Sienko, *Inorg. Chem.* **1972**, *11*, 904–906.
[5] K. Takahashi, S. Kunii, *J. Solid State Chem.* **1997**, *133*, 198–200.
[6] E. L. Kerley, C. D. Hanson, D. H. Russell, *Anal. Chem.* **1990**, *62*, 409–411.
[7] H. Zhang, Q. Zhang, J. Tang, L. C. Qin, *J. Am. Chem. Soc.* **2005**, *127*, 2862–2863.
[8] H. Zhang, J. Tang, Q. Zhang, G. Zhao, G. Yang, J. Zhang, O. Zhou, L. C. Qin, *Adv. Mater.* **2006**, *18*, 87–91.
[9] A. E. Baranovskiy, G. E. Grechnev, A. V. Logosha, I. V. Svechkarev, V. B. Filippov, N. Y. Shitsevalova, O. J. Zogał, O. Eriksson, *Phys. Status Solidi C* **2006**, *3*, 229–232.
[10] M. Takeda, T. Fukuda, F. Domingo, T. Miura, *J. Solid State Chem.* **2004**, *177*, 471–475.
[11] J. M. Lafferty, *J. Appl. Phys.* **1951**, *22*, 299–309.
[12] B. J. Curtis, H. Graffenberger, *Mater. Res. Bull.* **1966**, *1*, 27–30.
[13] J. R. Rea, E. Kostiner, *J. Cryst. Growth* **1971**, *11*, 110–116.
[14] S. Otani, H. Nakagawa, Y. Nishi, N. Kieda, *J. Solid State Chem.* **2000**, *154*, 238–241.
[15] S. Otani, M. M. Korsukova, T. Mitsuhashi, N. Kieda, *J. Cryst. Growth* **2000**, *217*, 378–381.
[16] X. D. Zhao, X. Y. Liu, F. Lin, W. N. Liu, W. H. Su, *J. Alloys Compd.* **1997**, *249*, 247–250.
[17] B. Post, D. Moskowitz, F. W. Glaser, *J. Am. Chem. Soc.* **1956**, *78*, 1800–1802.
[18] V. V. Gurin, M. M. Korsukova, S. P. Nikanorov, I. A. Smirnov, N. N. Stepanov, S. G. Shulman, *J. Less-Common Met.* **1979**, *67*, 115–118.
[19] Q. Y. Zhang, J. Q. Xu, Y. M. Zhao, H. J. Xiao, P. L. Shu, *Adv. Funct. Mater.* **2009**, *19*, 742–747.
[20] M. Kamaludeen, I. Selvaraj, A. Visuvasama, R. Jayavel, *J. Mater. Chem.* **1998**, *8*, 2205–2207.
[21] V. Craciun, D. Craciun, *Appl. Surf. Sci.* **2005**, *247*, 384–389.
[22] R. K. Selvan, I. Genish, I. Perelshtein, J. M. C. Moreno, A. Gedanken, *J. Phys. Chem. C* **2008**, *112*, 1795–1802.
[23] H. Zhang, Q. Zhang, G. P. Zhao, J. Tang, O. Zhou, L. C. Qin, *J. Am. Chem. Soc.* **2005**, *127*, 13120–13121.
[24] J. R. Brewer, N. Deo, Y. M. Wang, C. L. Cheung, *Chem. Mater.* **2007**, *19*, 6379–6381.
[25] M. F. Zhang, X. Q. Wang, X. W. Zhang, P. F. Wang, S. L. Xiong, L. Shi, Y. T. Qian, *J. Solid State Chem.* **2009**, *182*, 3098–3104.
[26] M. F. Zhang, L. Yuan, X. Q. Wang, H. Fan, X. Y. Wang, X. Y. Wu, H. Z. Wang, Y. T. Qian, *J. Solid State Chem.* **2008**, *181*, 294–297.
[27] J. J. Teo, Y. Chang, H. C. Zeng, *Langmuir* **2006**, *22*, 7369–7377.
[28] T. Sugimoto, *Adv. Colloid Interface Sci.* **1987**, *28*, 65–108.
[29] R. L. Penn, J. F. Baneld, *Science* **1998**, *281*, 969–971.
[30] R. L. Penn, J. F. Baneld, *Geochim. Cosmochim. Acta* **1999**, *63*, 1549–1557.
[31] J. F. Baneld, S. A. Welch, H. Zhang, T. T. Ebert, R. L. Penn, *Science* **2000**, *289*, 751–754.
[32] R. L. Penn, A. T. Stone, D. R. Veblen, *J. Phys. Chem. B* **2001**, *105*, 4690–4697.

Received: October 18, 2009
Published Online: February 2, 2010

